Delamination Prediction and Non-local Averaging using a Composite Micro-Mechanical Model

Ala Tabiei*, Sandeep Medikonda*

Department of Mechanical and Materials Engineering, University of Cincinnati, Cincinnati, Ohio 45221, USA

Abstract

Inter-laminar delamination in laminated composites has been studied with the help of thickness-stretch shell elements using a 3-D material model and compared against the traditional plane-stress shell elements. A strain-rate and pressure dependent micro-mechanical material model using ply-level progressive failure criteria has been used to simulate the initiation and propagation of delamination. The material parameters of the non-linear resin have been determined using LS-OPT®. The numerical delamination growth has been qualitatively analyzed against the experimental C-scan images for multiple impact events on different composite plates. In addition, a non-local model with an isotropic weight function has been implemented to work in conjunction with the composite micro-mechanical material model to alleviate strain softening typically seen in composite materials.

Keywords: Unidirectional composites; Micro-mechanical model; Continuum damage mechanics; Delamination; Non-local averaging; LS-DYNA®; LS-OPT

1. Introduction

Delamination, the principal model of failure of layered composites is the separation along interfaces, and is often considered to be one of the most dominant damage mechanism in the failure of composite laminates. Simulating and predicting delamination in composite materials is a challenging task, however it is critical in characterizing the overall response of Uni-Directional Composites (UDC). Typically, delamination failure is modelled in commercial finite element programs in the following ways:

1. Model a layer of shell or solid elements for each composite layer and bond the layers with a tiebreak contact.

2. Model a layer of shell of solid elements for each composite layer and bond the layers with cohesive elements.

Both these methods have their limitations as the use of solid element layers makes the simulations computationally expensive and the use of traditional shell elements doesn't quite represent the true mechanics of delamination accurately. Mainly because traditional shell element formulations often use a plane stress formulation (i.e., they do not account for the out-of-plane stress of σ_{33}). In addition, using tiebreak contacts with shell layers also triggers an un-realistic chain reaction of failure.

Arguably the fastest, most robust and efficient shell element formulation, which is usually the default element type in most commercial finite element codes, is based on the work of Belytschko, Lin and Tsay [1]. At its core this element formulation depends on the Reissner-Mindlin kinematic assumption which states that a plane section, originally normal to the mid-surface, remains plane and unstretched while allowing for shear deformations to occur. However, in addition to the zero thru-thickness stress limitation discussed above, these element types also need a modified constitutive law which corrects for the strain in the thickness direction. Since the early 1990's, there have been numerous attempts to formulate shell elements accounting for through-thickness deformation. Works of Simo et al. [2], Parish [3], Hauptmann and Schweizeroff [4] and Doll et al. [5]

demonstrate some of many contributions in the area of solid-shell element formulations. Büchter and Ramm [6], [7], El-Abbasi and Meguid [8], Betsch et al. [9] and Bischoff [10] have further enhanced the work to be applied for thin shells by solving the problem of strong thickness locking.

Cardoso's [11] work in particular overcomes the limitations of the Belytschko, Lin and Tsay formulation by relaxing the 'unstretched' Reissner-Mindlin assumption and allowing for a linear strain variation through the thickness as shown in Figure 1. This creates additional degrees of freedom which allows for loading on the surface of a shell element and would require a 3-D constitutive law in addition to preserving the advantages of the Belytschko, Lin and Tsay formulation. These type of shell elements have conventionally been used in sheet metal forming applications, where the presence of normal stresses in the thickness direction has been observed to improve the accuracy of the solution.
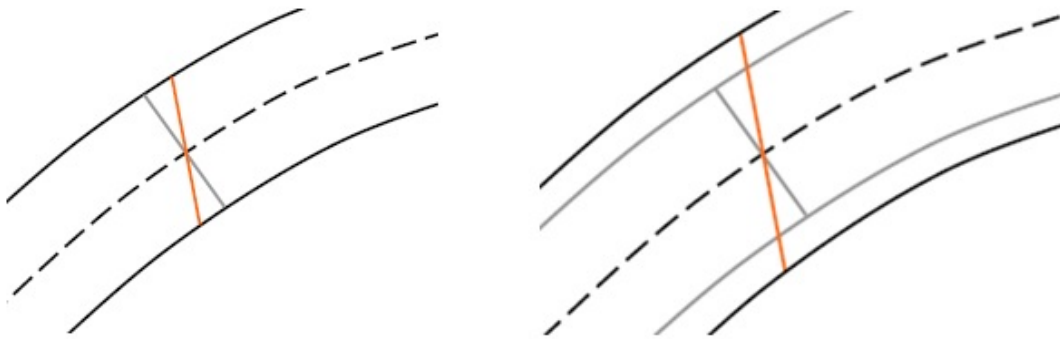
Figure 1: Traditional shell vs Thru-thickness shell

It is generally acknowledged that finite elements models with a fine mesh (smaller element size) yield more accurate results [12], [13]. However, this is no longer the case for strain-softening materials. Numerical studies have shown that the results in strain-softening materials are essentially dependent on the finite element mesh [14]–[16]. This complication is well known (Belytschko et al. [17], Larsy et al. [18]), and any type of strain localization phenomena (failure, in-elasticity, damage), will tend to localize in the smallest element of the finite element mesh. In other words, the smallest element in the mesh will tend to fail/erode before other elements. Also, finer the mesh, the energy dissipated by the numerical model decreases and tends to extremely low values, sometimes even to zero. Hence, the uniqueness of the solution with respect to the mesh size is lost, which is quite troubling from a numerical standpoint.

Different remedies addressing this problem have been presented in the open literature and can be classified into different categories/approaches. Cohesive crack models/Cohesive zone models (CZM) [19]–[21], Crack Band Model [22]–[24], Regularized differential (gradient-enriched) formulations [25]–[27] and Regularized integral formulations [28]. The current work focuses on studying the effect of integral nonlocal formulations on micro-mechanical composite models. These formulations abandon the classical assumption of locality and define stress at a point to be dependent not only on the state variable (usually strain, damage) at that point but also on a distribution of the state variable in a vanishing region around the point [29] and are fairly easier to work with in comparison to the differential formulations.

2. Micro-mechanics of the uni-directional composite (UDC)

The representative volume cell (RVC) used to develop the micro-mechanical relations is shown in figure (1). This RVC is the same as the one originally proposed by Pecknold and Rahman [30] and further used in various micro-mechanical models by Tabiei et al. in [31], [32], [33] and Medikonda et al. [34], [35]. However, for completeness the micro-mechanics relations are briefly discussed here. The unit cell is divided into three sub-cells: one fiber sub-cell, denoted as f, and two matrix sub-cells, denoted as M_A and M_B respectively. The

effective stresses in the RVC are determined from the sub-cell values by combining 2 material parts: material part *A* consists of the fiber sub-cell *f* and the matrix sub-cell *M_A*, and material part *B* consists of the remaining matrix *M_B* using the iso-strain boundary conditions for all the directions. The dimensions of the unit cell are 1 × 1 unit square. The dimensions of the fiber and matrix sub-cells are denoted by W_f *and* W_m respectively as shown in Figure 2 and defined as shown below:

$$W_f = \sqrt{V_f} \ ; \quad W_m = 1 - W_f \qquad\qquad \text{..... (1)}$$

where, V_f is the fiber volume fraction.
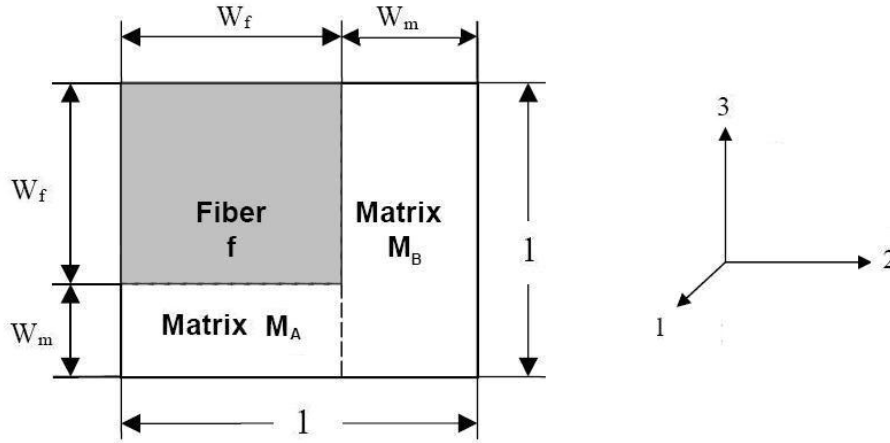
Figure 2: A representative volume cell of unidirectional fiber reinforced polymer composite

Visco-plastic constitutive relations based on modified Bodner-Partom state variable model, initially proposed by Goldberg et al. [36] and further enhanced by Zheng et al. [37] have been used to represent the matrix sub-cells *M_A* and *M_B*. The full details of the model can be found in these references, however for completeness only the incremental form of those equations are given below.

$$d\varepsilon_{ij}^I = \left(2D_0 \exp\left[-\frac{1}{2}\left(\frac{Z}{\sigma_e} \right)^{2n} \right]\left(\frac{S_{ij}}{2\sqrt{J_2}} + \alpha\delta_{ij} \right) \right)dt \qquad\qquad \text{..... (2)}$$

$$de_e^I = \sqrt{\frac{2}{3}de_{ij}^I de_{ij}^I} \ ; \qquad\qquad\qquad \text{..... (3)}$$

$$\text{where, } de_e^I = d\varepsilon_{ij}^I - d\varepsilon_m^I \ \& \ d\varepsilon_m^I = (d\varepsilon_{11}^I + d\varepsilon_{22}^I + d\varepsilon_{33}^I)/3$$

$$dZ = q(Z_1 - Z)de_e^I \qquad\qquad \text{..... (4)}$$

$$d\alpha = q(\alpha_1 - \alpha)de_e^I \qquad\qquad \text{..... (5)}$$

Stability against high strain increments has been ensured by implementing a 4-step Runge-Kutta integration scheme.

The constitutive relations of the fiber are initially assumed to behave as an elastic transversely isotropic material however these relations become orthotropic with damage evolution. The direct and shear stress stiffness matrices in terms of the properties of the fibers are:

$$[C_{fd}] = \begin{bmatrix} \dfrac{(1-d_1)E_1^f(1-v_{23}^f)}{(1-v_{23}^f-2v_{12}^fv_{21}^f)} & \dfrac{\sqrt{(1-d_1)E_1^f(1-d_2)E_2^fv_{12}^fv_{21}^f}}{(1-v_{23}^f-2v_{12}^fv_{21}^f)} & \dfrac{\sqrt{(1-d_1)E_1^f(1-d_3)E_2^fv_{12}^fv_{21}^f}}{(1-v_{23}^f-2v_{12}^fv_{21}^f)} \\[3ex] & \dfrac{(1-d_2)E_2^f(1-v_{12}^fv_{21}^f)}{(1+v_{23}^f)(1-v_{23}^f-2v_{12}^fv_{21}^f)} & \dfrac{(v_{23}^f+v_{12}^fv_{21}^f)E_2^f\sqrt{(1-d_2)(1-d_3)}}{(1+v_{23}^f)(1-v_{23}^f-2v_{12}^fv_{21}^f)} \\[3ex] Symm. & & \dfrac{(1-d_3)E_2^f(1-v_{12}^fv_{21}^f)}{(1+v_{23}^f)(1-v_{23}^f-2v_{12}^fv_{21}^f)} \end{bmatrix} \quad\text{….. (6)}$$

$$[C_{fs}] = \begin{bmatrix} G_{12}^f & 0 & 0 \\ & G_{23}^f & 0 \\ Symm. & & G_{o12}^f \end{bmatrix} \quad\text{….. (7)}$$

Once the stresses in all the constituent sub-cells have been obtained, they are then combined using the iso-strain boundary conditions to obtain the effective stresses of the RVC.

$$\sigma_{11}^{RVC} = W_f^2\sigma_{11}^f + (1-W_f^2)\sigma_{11}^R \quad\text{….. (8)}$$

$$\sigma_{22}^{RVC} = W_f^2\sigma_{22}^f + (1-W_f^2)\sigma_{22}^R \quad\text{….. (9)}$$

$$\sigma_{33}^{RVC} = d_z\left[W_f^2\sigma_{33}^f + (1-W_f^2)\sigma_{33}^R\right] \quad\text{….. (10)}$$

$$\sigma_{12}^{RVC} = W_fV_{s4}\sigma_{12}^f + (1-W_fV_{s4})(1-d_4)\sigma_{12}^R \quad\text{….. (11)}$$

$$\sigma_{23}^{RVC} = d_{yz}\left[W_fV_{s5}\sigma_{23}^f + (1-W_fV_{s5})(1-d_5)\sigma_{23}^R\right] \quad\text{….. (12)}$$

$$\sigma_{31}^{RVC} = d_{zx}\left[W_fV_{s4}\sigma_{31}^f + (1-W_fV_{s4})(1-d_6)\sigma_{31}^R\right] \quad\text{….. (13)}$$

Since, the use of iso-strain boundary conditions for shear isn't quite realistic in a physical sense [34], different ad-hoc shear volume fraction coefficients, V_{s4} and V_{s5}, for the in-plane and transverse shear have been introduced and have values quite lower than the volume fraction of the fibers. Damage parameters d_i, $i = 4,\ 5,\ 6$, represent the damages imposed on the matrix material and affect only the shear stresses of the resin. Damage parameters d_i, $i = 1,...,6$, in the above relations follow progressive failure models and are discussed in the following section.

Damages d_z, d_{yz} and d_{zx} are introduced by the inter-laminar delamination model use the same criteria as MAT161 in LS-DYNA. Delamination initiation, which is a consequence of the quadratic interaction between the out-of-plane stresses of a lamina and is assumed to be mainly a lamina failure is given by the following relation:

$$S^2\left\{\left(\frac{E_3\langle\varepsilon_{33}\rangle}{S_{3t}}\right)^2 + \left(\frac{G_{23}\gamma_{23}}{S_{230}+S_{SR}}\right)^2 + \left(\frac{G_{31}\gamma_{31}}{S_{310}+S_{SR}}\right)^2\right\} - r^2 = 0 \quad\text{….. (14)}$$

It has to be noted here that the elastic material parameters specified in Equation (14) correspond to the macro-properties of the lamina, which are back calculated from the stiffness matrix assembled for the RVC (Equations (8-13)) as discussed by Qu and Cherkaoui [38].

Once the damage threshold has been reached, delamination failure is introduced using a Weibull damage function in a progressive manner.

$$d_{lam}^{(n+1)} = \max\left\{1 - \exp\left[\frac{1}{m_d}\left(1 - r^{m_d}\right)\right], d_{lam}^n\right\} \quad\text{….. (15)}$$

Depending on the opening or closing of the damage surfaces, Equation (15) is used to subsequently reduce d_z, d_{yz} and d_{zx}. Note that the presence of friction is also accounted with the help of the Coulomb-Mohr theory when

the damaged/delaminated surfaces are "closed" [32], [39]. The advantage of using a CDM based failure model is that it can effectively simulate failure under all conditions such as opening, closure and sliding of failure surfaces.

3. Damage and Non-local formulation

Progressive damage models with strain softening behavior have traditionally been observed as good remedies to significantly improve damage predictions [40]–[42]. The first well known CDM model was developed by Matzenmiller, Lubliner and Taylor (MLT) [43]. Works of Williams and Vaziri [44], [45] have later reviewed and suggested improvements to the MLT model. Damage growth in the current work is hence based on different variations of the Weibull distribution functions. Fibers are assumed to govern the behavior of the composite in direct loading, while the matrix is assumed to dictate the response in the shear directions.

$$d_k^{n+1} = \max \left\{ 1 - \exp \left[-\frac{1}{me} \left(\frac{E_k^{damaged} \varepsilon_{ij}}{\sigma_{ij}^{t|c}} \right)^{m_k} \right], \ d_k^n \right\} \qquad \text{..... (16)}$$

where, $ij = 12, 23 \ or \ 31$ *and* $k = 1, 2 \ or \ 3$

$$d_k^{(n+1)} = \max \left\{ 1 - \exp \left[-\left(\frac{|\varepsilon_{ij}|}{\varepsilon_{km}} \right)^{m_s} \right], \ d_k^{(n)} \right\} \qquad \text{..... (17)}$$

where, $ij = 12, 23 \ or \ 31$ *and* $k = 4, 5 \ or \ 6$

Where, $t|c$ denotes tension or compression. When a positive strain is detected, the parameters for tension are utilized otherwise the parameters provided for compression are used. $\sigma_{ij\ t|c}^{fud}$ is the undamaged stress in the fibers and when the damage d_1 reaches 0.01 in tension, the finite element is considered to be totally failed. Damages d_2, d_3 are constrained to not fall below 0.1 and the shear damages below 0.2. The primary reason for constraining the damages is to account for the numerical instabilities that arise when stress in an element goes to zero.

For the non-local approach, the formulation proposed by Andrade et al. [46] has been incorporated in the 'urmathn' subroutine to work with the user-defined material model (UMAT) in LS-DYNA (Figure 3). The nonlocal approach consists of calculating its nonlocal counterpart obtained by weighted averaging over a spatial neighborhood of each point under consideration. Hence in a domain field *V*, the corresponding nonlocal damage variable is defined as:

$$\bar{d}_k(\boldsymbol{x}) = \int_V \beta(\boldsymbol{x}, \boldsymbol{\xi}) d_k(\boldsymbol{\xi}) dV(\boldsymbol{\xi}) \qquad \text{..... (18)}$$

Where, $\beta(\boldsymbol{x}, \boldsymbol{\xi})$ is a given nonlocal operator. In an infinite body, the weight function depends only on the distance between the 'source point', $\boldsymbol{\xi}$, and the 'target' point, $\boldsymbol{x}$, and is given by the following relation:

$$\beta(\boldsymbol{x}, \boldsymbol{\xi}) = \frac{\alpha(\boldsymbol{x}, \boldsymbol{\xi})}{\int_V \alpha(\boldsymbol{x}, \boldsymbol{\xi}) dV(\boldsymbol{\xi})} \qquad \text{..... (19)}$$

It should be noted that the weighing function $\alpha(\boldsymbol{x}, \boldsymbol{\xi})$ is a monotonically decreasing non-negative function of the distance $r = \|\boldsymbol{x} - \boldsymbol{\xi}\|$. Typically, a Gaussian distribution is considered as the weight function and is given by the following relation:

$$\alpha(\boldsymbol{x}, \boldsymbol{\xi}) = \exp \left(-\frac{\|\boldsymbol{x} - \boldsymbol{\xi}\|^2}{2L^2} \right) \qquad \text{..... (20)}$$

Where L, is a parameter reflecting the internal length of the nonlocal continuum and should be experimentally determined.

From a numerical implementation point of view, the non-local value of the damage variable can be calculated by using the damage from the previous time step 'n' (Equation (16)) and the Gaussian quadrature integration rule.

$$\bar{d}_k^n = \sum_{j=1}^{npg_i} w_j J_j \beta_{ij} d_k^n \qquad \text{..... (21)}$$

Where, β_{ij} is the nonlocal operator that relates the Gauss points i and j located at global coordinates x and ξ respectively. In additions the quantities w_j and J_j are the Gaussian weights and Jacobian evaluated at Gauss point j. Lastly, npg_i is the number of Gauss points that lie inside the nonlocal volume of interaction from point i. It should be noted that the factors w_j, β_{ij} and J_j are merely geometrical in nature and they depend on the finite element mesh itself rather that the constitutive model (UMAT). Hence, these factors only need to be calculated once, at the start of a simulation. The key part of the implementation lies in calculation of the nonlocal penalty factor K^{nl}:

$$K^{nl} = \frac{\bar{d}_k^n}{d_k^n} \qquad \text{..... (22)}$$

which is then used to calculate the nonlocal value of the damage variable at the current time step $d_k^{(n+1)*}$

$$d_k^{(n+1)*} = K^{nl} d_k^{n+1} \qquad \text{... (23)}$$

Lastly, instead of the local value of the damage the updated nonlocal value can be used in reducing the stiffness of lamina.

$$E_k^{damaged} = (1 - d_k^{(n+1)*}) E_k^{un-damaged} \qquad \text{..... (24)}$$

The reduced values of the stiffness are then used to calculate the effective stresses of the representative volume cell discussed in the previous section. Note that, the drawback of accessing the neighboring integration points at once is overcome by adopting a strategy that saves and uses information of the damage variable from a previous time step. The disadvantage of such as assumption is that it necessitates small time steps for enough accuracy. However, since the explicit time integration scheme of LS-DYNA naturally requires a very small-time step (less than the critical time step ($\Delta t \leq 2/\omega_{max}$) to guarantee stable solutions this condition is easily met. It is worth mentioning that LS-DYNA does offer the option of using nonlocal formulations through the keyword *MAT_NONLOCAL, however this option is limited to the use of very few elastoplastic models, nonetheless user-defined material models.
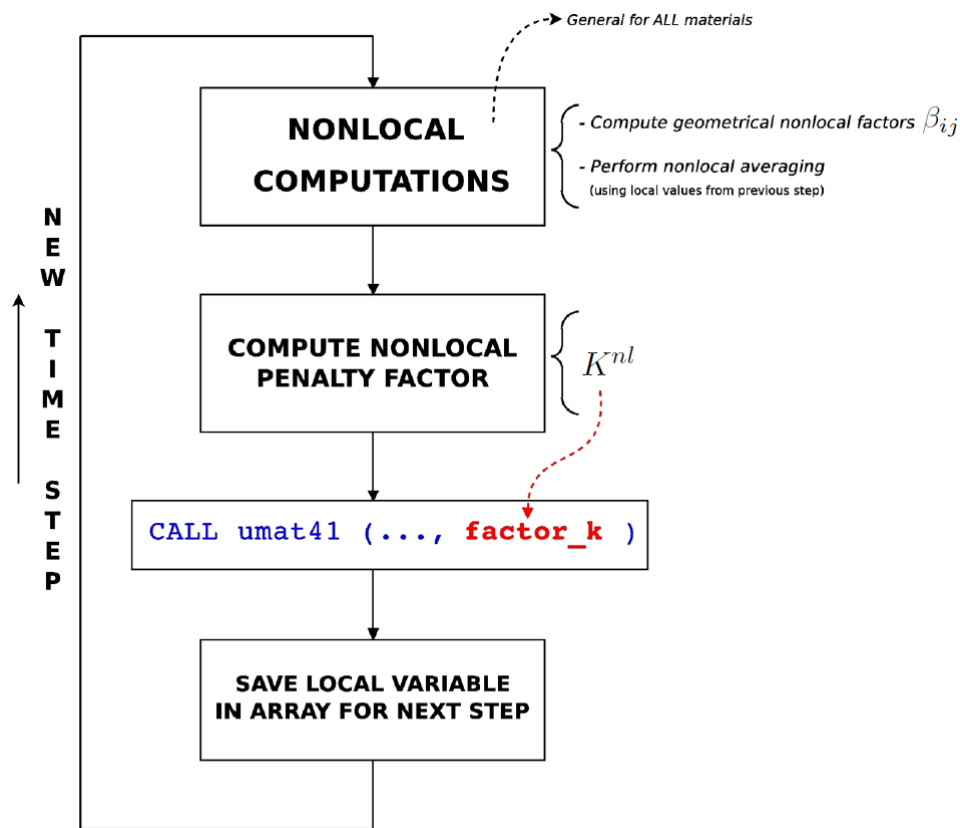
Figure 3: Schematic flowchart illustrating the implementation of nonlocal strategy in LS-DYNA
[46]

4. Numerical Results and Discussion of Inter-laminar delamination

Impact events on T800H/3900-2 CFRP plates have been chosen for verification. Since the current material model has been based on micro-mechanics, there is a need to characterize the visco-plastic material parameters of the resin. However, it must be noted that the stress-strain responses that are necessary for the calculation of the viscoplastic parameters are not available directly in the literature. For the 3900-2 resin, these have been back-calculated based on the work Tabiei and Babu [47]. In their work, Tabiei and Babu presented the visco-plastic parameters for a resin material model based on the Goldberg-Stouffer relations. A standalone material model based on these relations and the material parameters has been developed as a VUMAT in LS-DYNA and stress-strain curves have been generated for 3 strain rates in the tensile (0.1/s, 1.4/s and 510/s) and shear (0.1/s, 1.76/s and 420/s) directions. The generated data has then been fit to the current resin material model using the LS-OPT software, the flow chart of which is shown in Figure 4.

LS-OPT [48] is a standalone optimization software that can be linked to any finite element code. It is particularly useful for the current case since it provides a simple interface to work with LS-DYNA. One popular use of LS-OPT is for calibrating material parameters. Parameter identification problems are non-linear inverse problems solved using optimization, in other words, the computed curve from LS-DYNA (dependent on parameters) is matched to an input curve. The two essential components involved in parameter identification are the optimization algorithm and the curve matching metric. The Sequential Response Surface Method (SRSM) is the recommended/default optimization algorithm used in parameter identification problems, the reader is directed to Stander et al. [48] for further details on this algorithm.

To calculate the mismatch between the target and the computed curve, an ordinate-based Mean Square Error (MSE) curve matching metric has been selected. For completeness, the underlying principle of this metric is

discussed here. Once the target stress-strain curves have been inputted as file histories, the mean squared residual error between the input data and the numerically generated data (based on a tensile and shear responses for various strain rates) has been calculated based on the equation given in Equation (25) and subsequently minimized.

$$MSE(\mathbf{x}) = \frac{1}{N}\sum_{i=1}^{N} W_i \left(\frac{f_i(\mathbf{x}) - G_i}{s_i} \right)^2 = \frac{1}{N}\sum_{i=1}^{N} W_i \left(\frac{e_i(\mathbf{x})}{s_i} \right)^2 \rightarrow min.$$

where,

$f_i(\mathbf{x})$: simulation response as a function of variable vector **x**

G_i: target value   ….. (25)

W_i: weighting factor

s_i: normalization factor (absolute max. value of each curve)

N: no. of points

$e_i(\mathbf{x})$: error at each point
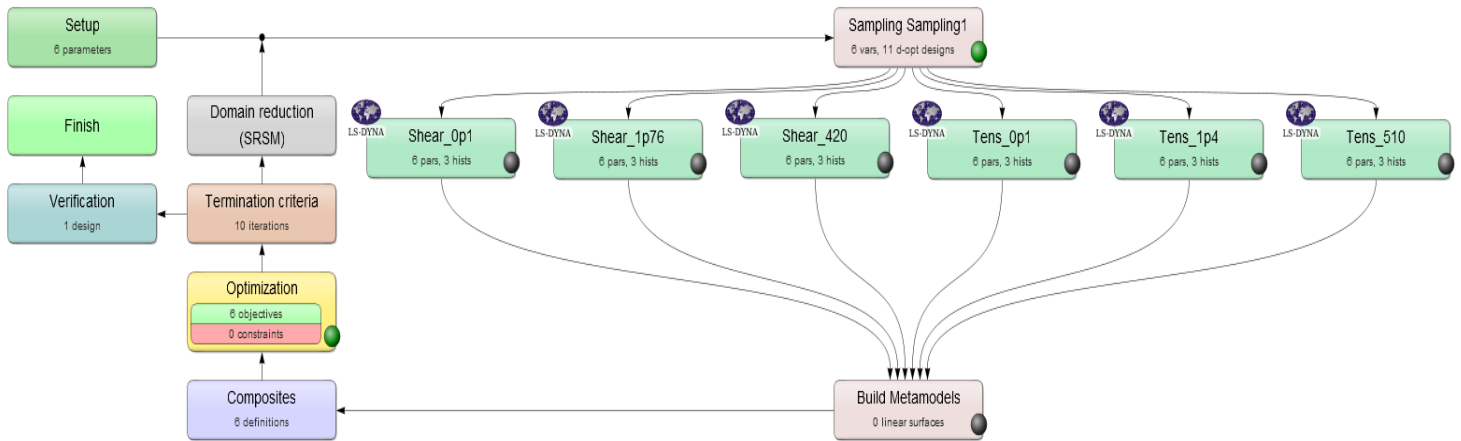
Figure 4: LS-OPT Flowchart for resin material parameter calculation

It must be noted that the backend solver has been built using intel compilers and the UMAT (User MATerial) subroutine in LS-DYNA, based on the constitutive relations discussed in section 2. As inputs for LS-OPT, parameterized single element input decks with tensile and shear boundary conditions have been used with the respective strain rate specified. As it can be observed from Figure 6, the fitted response of the 3900-2 resin is quite close to the target data specified.

Table 1 lists all the visco-plastic parameters obtained for the 3900-2 resin from LS-OPT. The above discussion and the use of an optimization tool (LS-OPT) presents a simplified way of characterizing the visco-plastic material once the experimental data is available.

Resin	$E_0(GPa)$	v_m	$D_0(1/s)$	n	$Z_0(MPa)$	$Z_1(MPa)$	q	α_0	α_1
3900 - 2	3.5	0.34	$1*10^6$	1.5	188.447	464.172	237.143	0.284	0.01

Table 1: Material Constants for the 3900-2 Resin

The impact event on CFRP plates made of T800H/3900-2 fiber/resin system with a laminate stacking sequence of $[45/90/-45/0]_{3s}$ and total thickness of 4.65 mm has been simulated using the current material model in LS-DYNA. These experimental results were originally obtained by an extensive investigation of out-of-plane impact loading of composite test coupons by Delfosse [49] and were used by Williams and Vaziri et al. [45] to evaluate the predictive capability of a plane-stress CDM based model for composite materials that they implemented in LS-DYNA.

The goal of this study is to qualitatively predict the delamination and compare it with the experiments as reported in Williams et al. [45]. The test coupon consists of a simply supported 76.2 mm by 127 mm plate impacted by a hemispherical steel impactor ($25.4\,mm$ in diameter), which in the numerical computation is treated as rigid body. The FE model is shown in Figure 5.
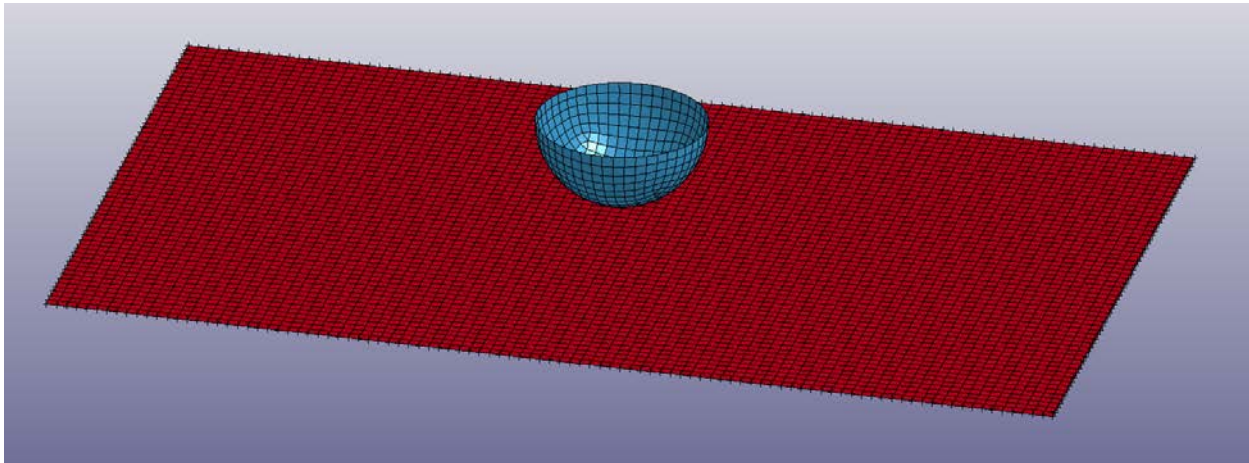
Figure 5: A full model view of the T800H/3900-2 CFRP laminate
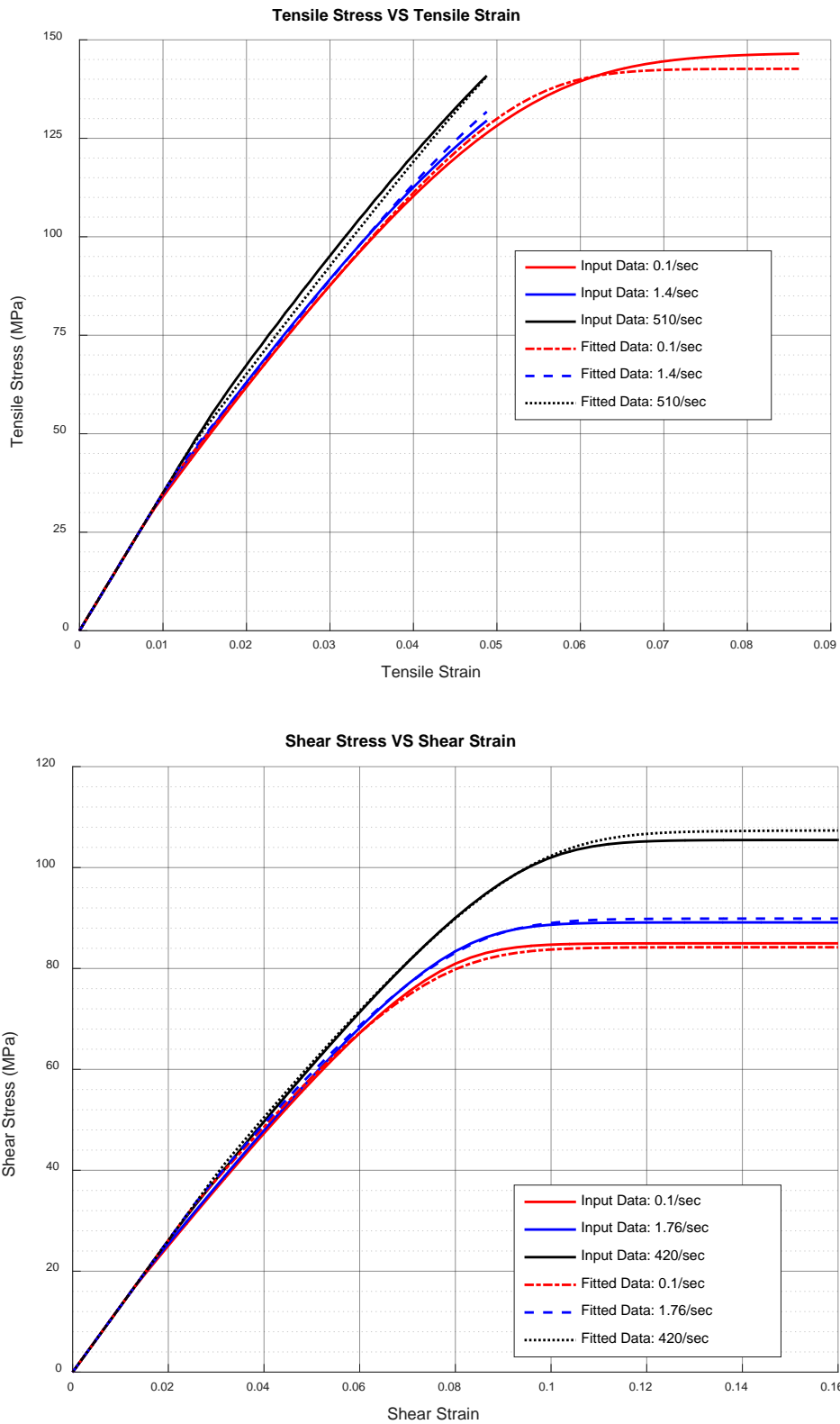
Figure 6: Tensile and Shear stress fitted curves for 3900-2 resin

The CFRP plate consists of 24-thru thickness integration points with each integration point representing a layer of the laminate stacking sequence $[45/90/-45/0]_{3s}$. In addition to the visco-plastic properties of the resin specified in Table 1, the remaining material properties needed to carry out the simulations have been specified in Table 2.

V_f	$\dot{\varepsilon}_o\ (s^{-1})$	$E_1(GPa)$	ν_{12}	$X_t(Mpa)$	$X_c(Mpa)$	$E_2(GPa)$	ν_{23}
0.51	1×10^{-3}	294	0.25	5490	1600	19.6	0.25
$\sigma_{2t}(Mpa)$	$\sigma_{2c}(Mpa)$	$G_{o12}(GPa)$	$G_{23}(GPa)$	a_{s4}	ε_{4m}	ε_{5m}	V_{s4}
400	255	20	7.26	0.010	0.14	0.14	0.100
V_{s5}	$a_G(GPa)$	b_t	b_c	$S_{3t}(MPa)$	$S_{230}(MPa)$	$S_{310}(MPa)$	φ (deg.)
0.200	0.800	1.36	1.00	79	86	64	10
S	m_d						
1.0	2						

Table 2: Fiber and damage properties for the T800H/3900-2 lamina

Figure 7 qualitatively compares the predictions of projected inter-laminar delamination to the C-scan images of delamination growth for the low mass impact events provided in [45]. The box drawn around the numerical results highlights the location of the plate boundaries relative to the part of the plate modelled. Observing the results presented in Figure 7, the following comments can be made:

a) The total delamination area looks smaller as compared to the experiments when both sets of images in each figure (numerical and C-scan) are set to the same scale. The reasons for these can be attributed to two possibilities.

   i. First, the C-scan images indicate matrix failure and delamination in the complete laminate. In other words, they show the cumulative delamination in all layers. The numerical results on the other hand are shown only for the interface that experiences the maximum amount of delamination (which is the bottom most interface for the current cases), this is due to a limitation in the post-processing capabilities for shell elements.

   ii. Secondly, the delamination model used in the current study uses a stress-based criterion, where the inter-laminar and out-of-plane stresses were used to predict the initiation and growth of delamination. These models have traditionally been proven to be effective in capturing the initiation of delamination, but aren't as effective in capturing the scale effects. Davies and Zhang [50] and subsequently Tabiei and Babu [32] have shown that the stress-based delamination criteria under predict the delamination area.

b) The shape of the delamination however looks quite identical in both the cases as compared to the experiments.

c) The delamination areas predicted by the thickness-stretch element models seem to be identical as compared to the areas predicted by the plane-stress shell element models.
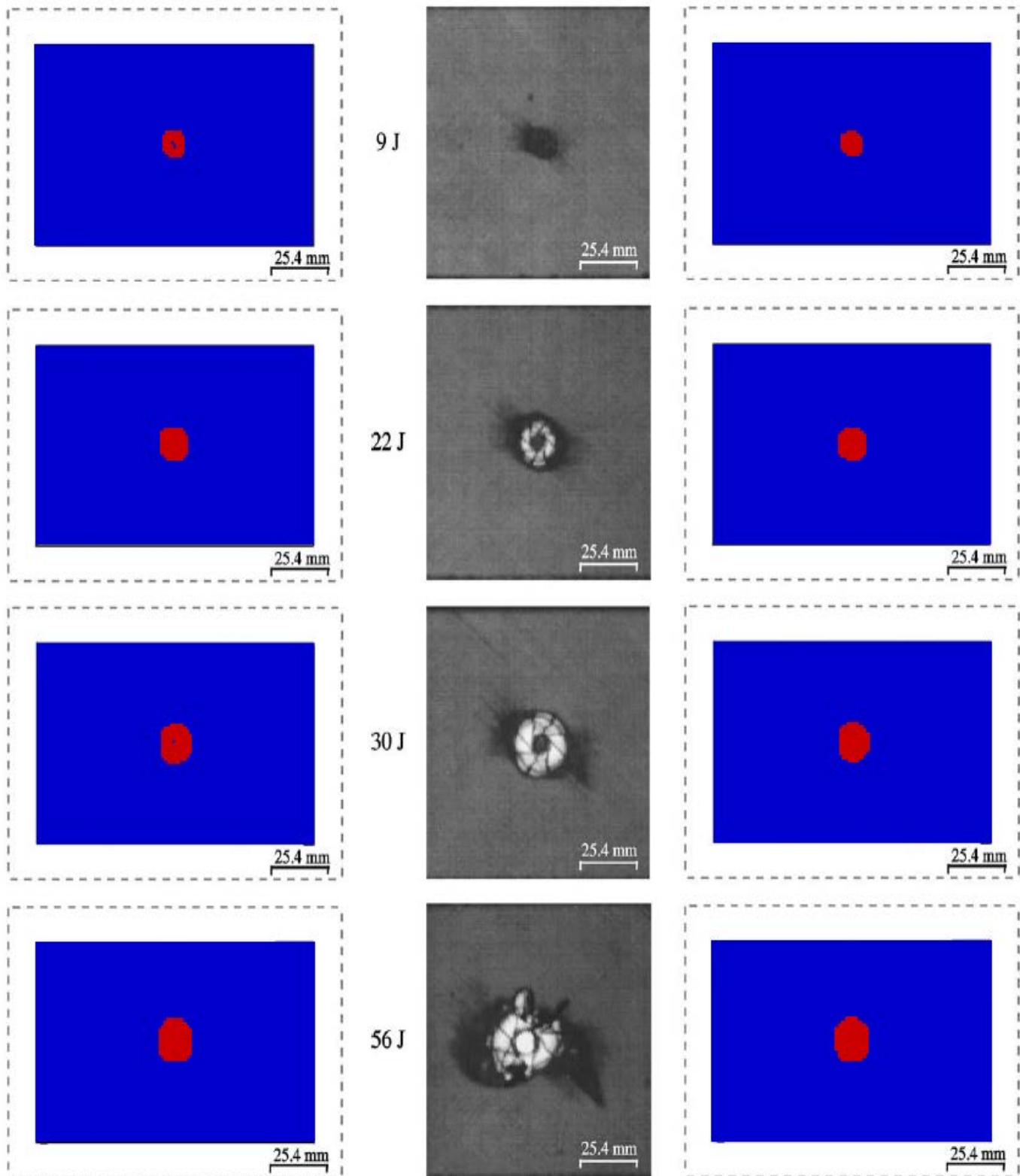
Figure 7: Comparison of the delamination damage and experimental C-scan images on a T800H/3900-2 CFRP plate. Numerical results obtained using plane-stress shell elements have been shown on the left and the thickness-stretch shell elements on the right.

To further understand the effect of Z-Stress on delamination behavior, it is important to consider the effect of each term on the left-hand side of equation (14). In this equation, the first term accounts for the contributions

from Z-Stresses, the second term for the YZ-Stresses and the last term for the ZX-Stresses of the lamina. The contributions of each of these stresses can be better understood from Figure 8-Figure 10.

The following comments can be made on the results presented in these figures.

a) A contribution of the Z-Stresses has been seen in the model run using thickness-stretch shell elements, however this is small compared to the contribution from the YZ and ZX-Stresses, i.e., the number of red-spots are fewer. Which explains the identical shapes observed in Figure 7. It must be noted that as the total value of these terms goes beyond a value of 1, damage is introduced into the model and the load bearing capacity of the lamina in Z, YZ and ZX directions is reduced.

b) As expected, for the model run with traditional plane-stress shell elements, the Z-Stress contribution is zero and the total damage is completely dominated by the YZ and ZX-Stress contributions in the delamination criteria.

c) Despite being small, the contribution of Z-Stresses in predicting delamination cannot be completely ignored. These stresses have been observed to have contributed nearly 6% of the total delamination damage at the point of initiation.
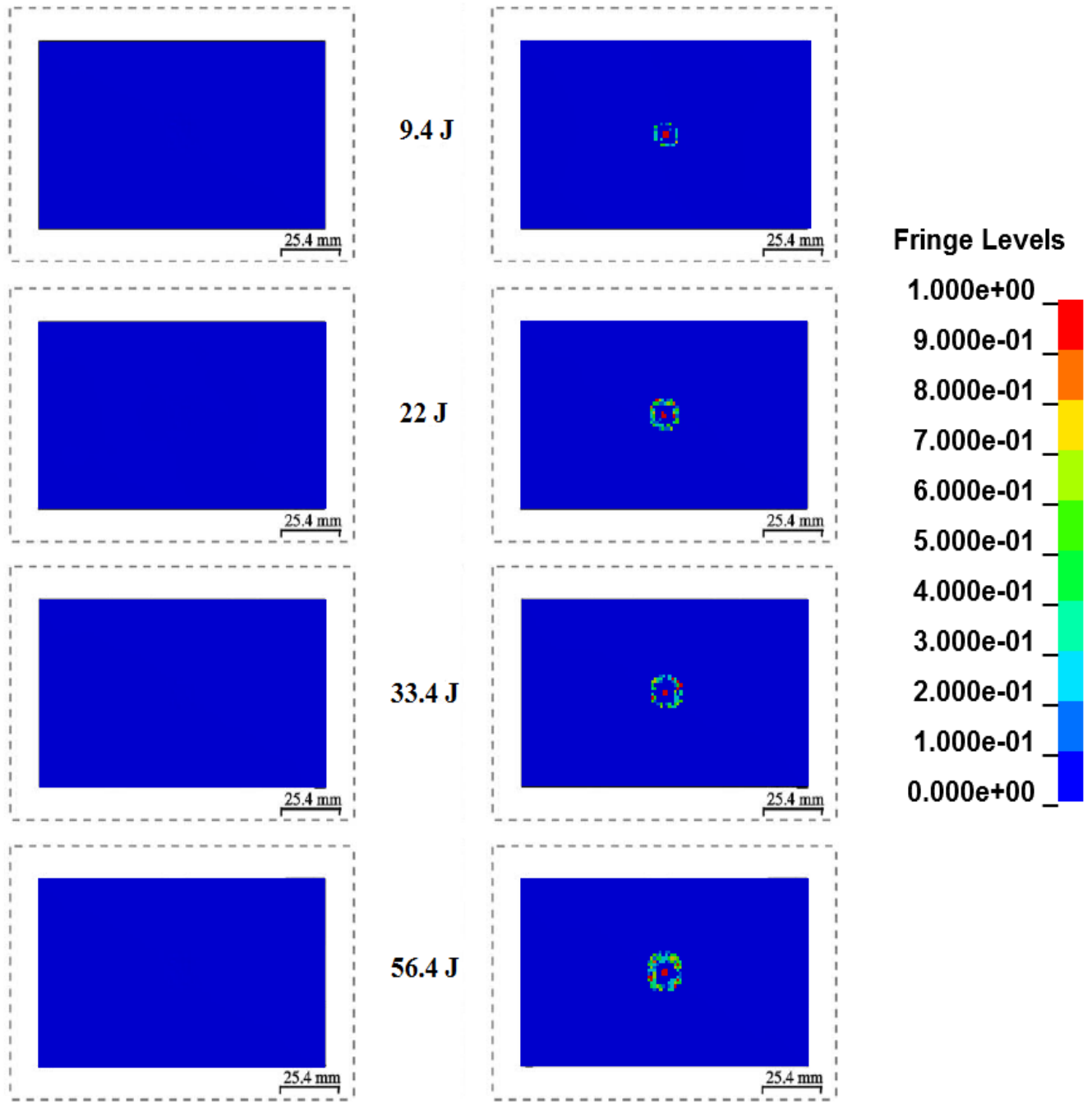
Figure 8: Contribution of Z-Stresses in the calculation of delamination for the bottom layer. Numerical results obtained using plane-stress shell elements have been shown on the left and the thickness-stretch shell elements on the right.
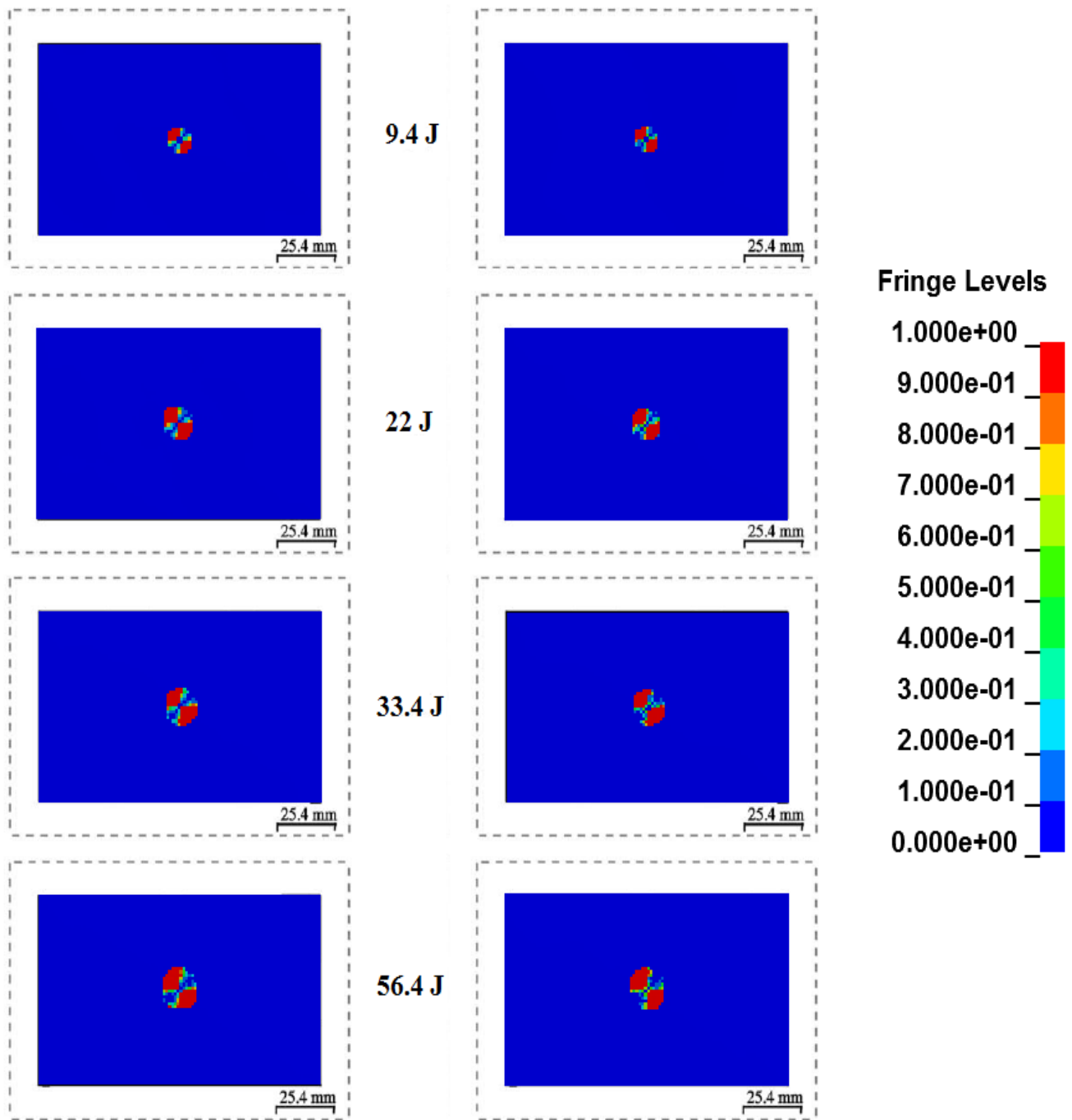
Figure 9: Contribution of YZ-Stresses in the calculation of delamination for the bottom layer. Numerical results obtained using plane-stress shell elements have been shown on the left and the thickness-stretch shell elements on the right.
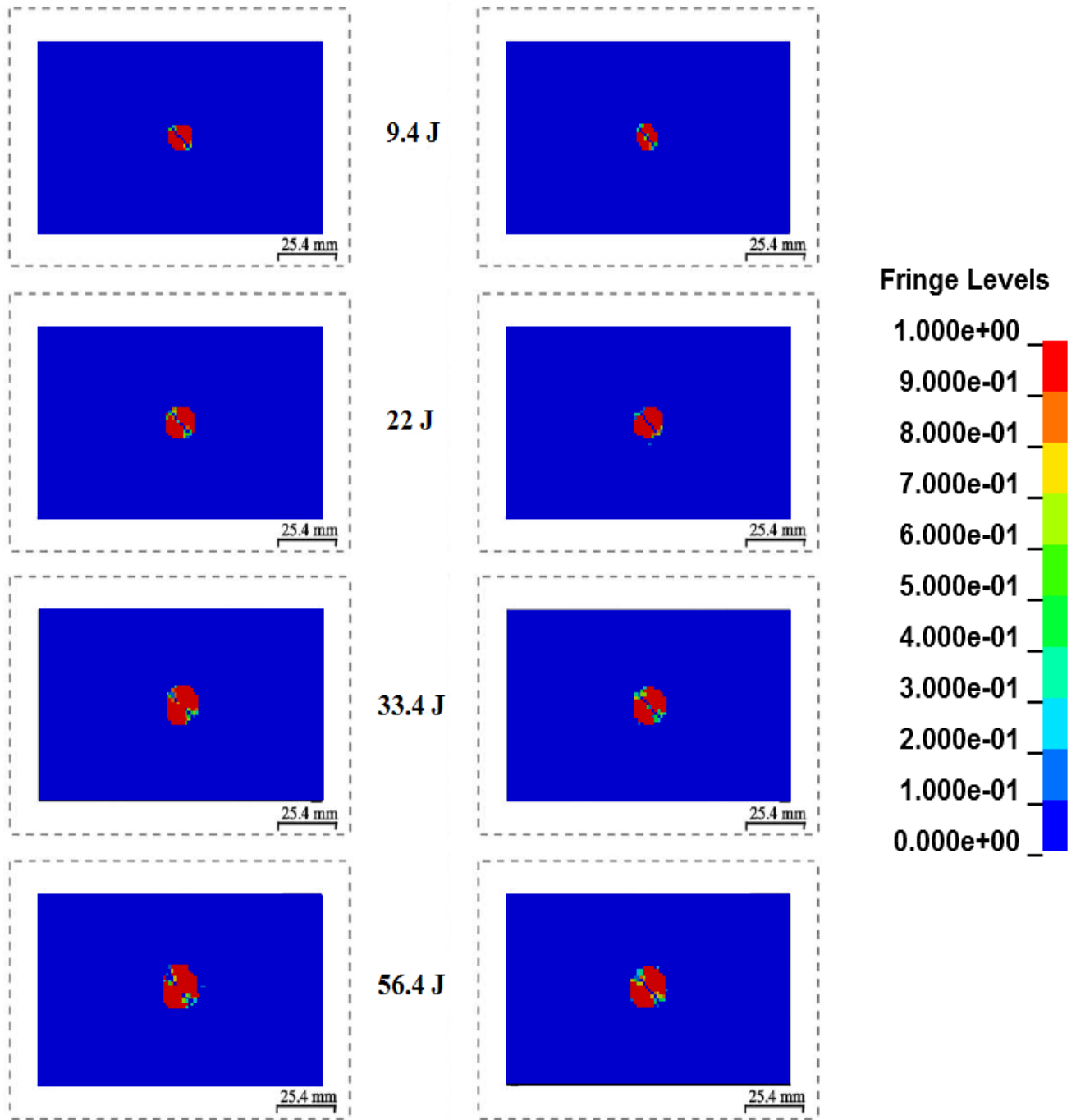
Figure 10: Contribution of ZX-Stresses in the calculation of delamination for the bottom layer. Numerical results obtained using plane-stress shell elements have been shown on the left and the thickness-stretch shell elements on the right.

5. Non-local Results and Discussion

To test the non-local technique, it has been implemented along with the micro-mechanical material model discussed in the previous sections and applied on a tensile dog-bone specimen, commonly used in the experimental determination of the properties of composites. The dimensions of the specimen are shown in Figure 11.
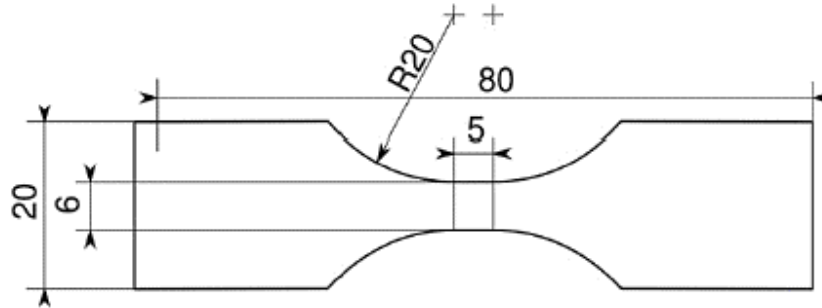
Figure 11: Tensile Dog-bone Specimen [46]

The FE models have been built for 3 mesh sizes. It should be noted that the mesh size has been only significant increased for the curved part of the specimen since this is the primary area of interest. The symmetry in the specimen has been taken into consideration and hence only a quarter of the model has been modeled to reduce computational effort.

The material properties of E-glass/Epoxy discussed in Medikonda et al. [35] have been used here. Note that one end of the specimen has been fixed and the other end of the specimen is being pulled by 1.2 mm. Initially, the models have been run without calling the non-local routine and the results of local damage in the pull direction in the end deformed state have been presented in Figure 12. As expected, strain tends to localize in a few elements for these cases and as a result the material damages completely in those regions. In addition, note that the maximum allowable damage in the fiber direction (d_1) has been constrained to 0.01 to account for numerical instabilities and element deletion has been turned off.

Results shown in Figure 13 correspond to the tensile tests carried out with the non-local formulation activated.
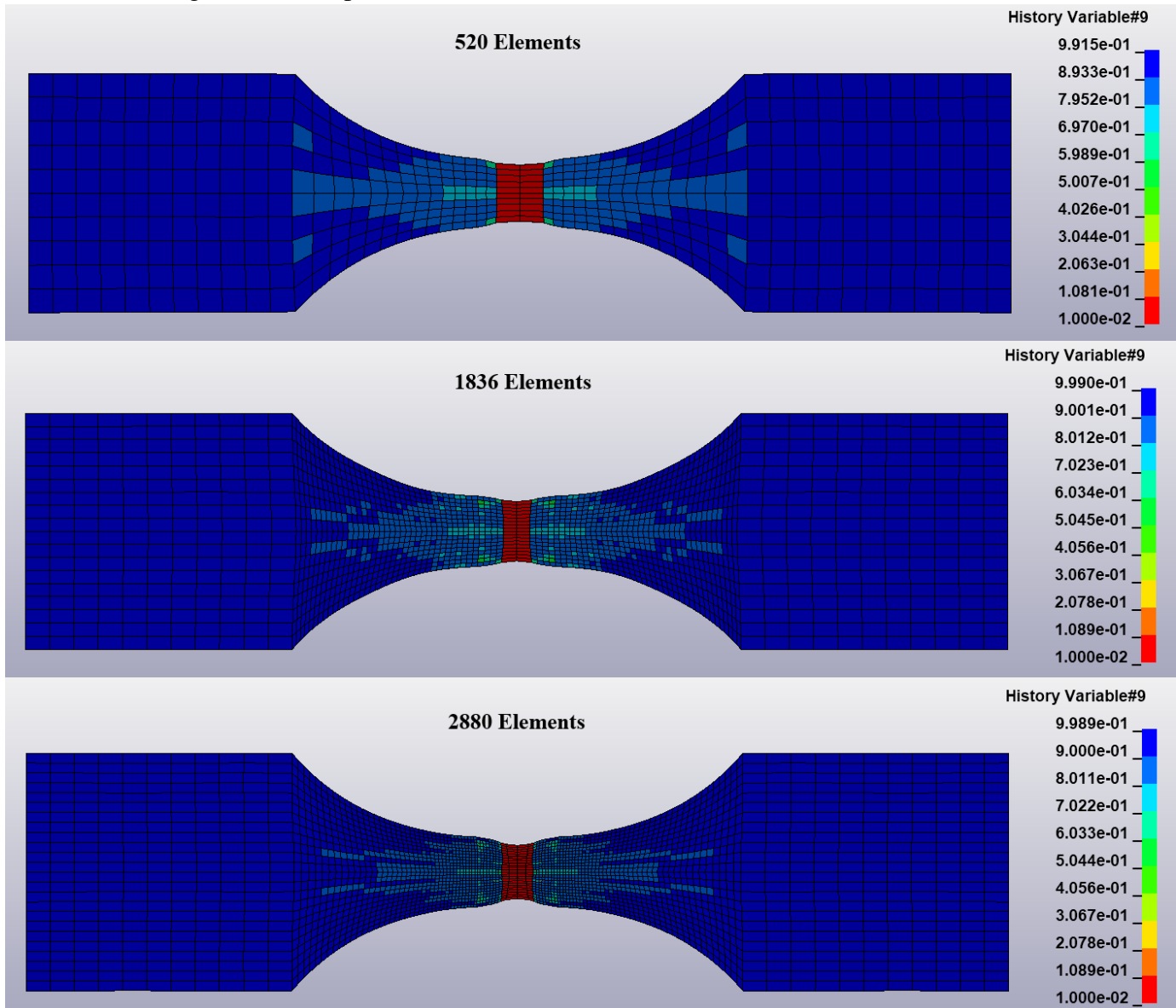
Figure 12: Local Damage in the Tensile Dog-bone Specimen for different mesh sizes

It is clearly seen that the non-local formulation prevents strain-localization and shows a more smeared effect of damage. It is important to note that the maximum damage (lower value shown in the figure) experienced by each model is different and for consistent comparison the fringe limits have been manually adjusted to correspond to the maximum damage experienced by the models in the figure (which is the model with most elements in this case).

As the no. of elements in the model increases, the damage distribution tends to become similar and the variation in the maximum amount of damage observed in each model, becomes quite less as well. Also, as expected with an increase in the mesh density, a smoother variation of damage has been observed.
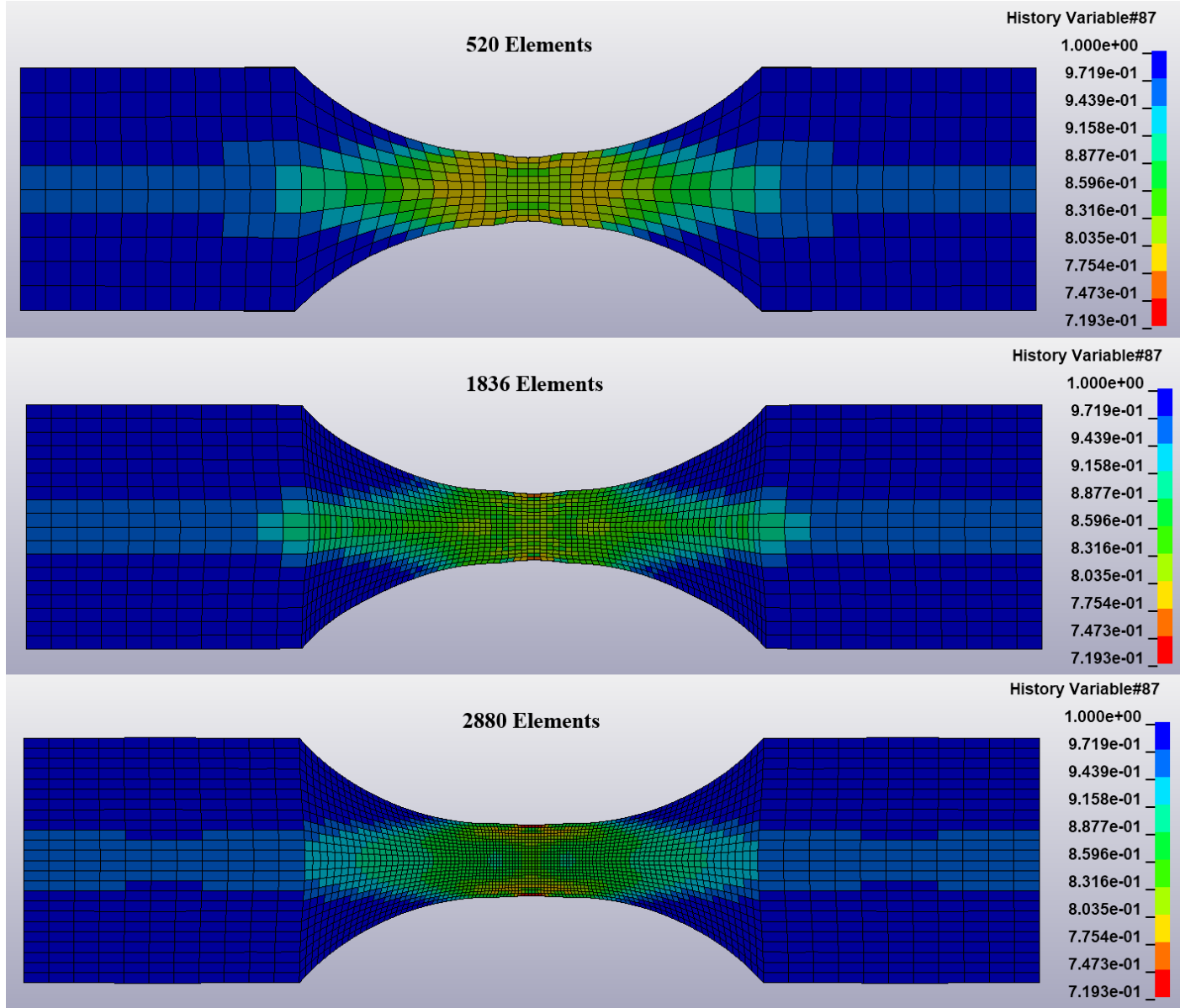
Figure 13: Non-local damage in the Tensile Dog-bone Speciment for different mesh sizes

6. Conclusions

A strain-rate dependent micro-mechanical material model has been developed in LS-DYNA (as a user-defined material UMAT), to study delamination damage growth in uni-directional composites using thickness-stretch shell elements and plane-stress shell elements under impact loading conditions. This is mainly done as, through-thickness stresses resulting from out of plane loadings, such as contact forces, are expected to either promote or inhibit delamination growth. The ability of thickness-stretch shell elements in using a 3-D constitutive law makes them an interesting option in studying delamination growth, especially when used in conjunction with a stress-based approach.

The strain-rate dependency is accounted with the help of the modified Bodner-Partom viscoplastic relations in the resin. A significant advantage of these relations is that they account for the contribution of the hydrostatic stresses in predicting the non-linear response, which is a well-known and crucial characteristic of polymers. The material parameters of the resin have been characterized by minimizing the mean square error in an optimization software (LS-OPT).

In addition, a nonlocal model has been coupled with a non-linear micro-mechanical composite material model and implemented with the UMAT. The non-local formulation has been designed to work with the progressive damage law of the constitutive model. Numerical analyses have been carried out on a tensile dog-bone specimen and the results have shown that the non-local strategy has been able to prevent the strain localization traditionally seen in strain-softening material models.

References

[1]   T. Belytschko, J. I. Lin, and T. Chen-Shyh, "Explicit algorithms for the nonlinear dynamics of shells," *Comput. Methods Appl. Mech. Eng.*, vol. 42, no. 2, pp. 225–251, 1984.

[2]   J. C. Simo, M. S. Rifai, and D. D. Fox, "On a stress resultant geometrically exact shell model. Part IV: Variable thickness shells with through-the-thickness stretching," *Comput. Methods Appl. Mech. Eng.*, vol. 81, no. 1, pp. 91–126, 1990.

[3]   H. Parisch, "A continuum-based shell theory for non-linear applications," *Int. J. Numer. Methods Eng.*, vol. 38, no. 11, pp. 1855–1883, Jun. 1995.

[4]   R. Hauptmann and K. Schweizerhof, "A systematic development of 'solid-shell' element formulations for linear and non-linear analyses employing only displacement degrees of freedom," *Int. J. Numer. Methods Eng.*, vol. 42, no. 1, pp. 49–69, May 1998.

[5]   S. Doll, K. Schweizerhof, R. Hauptmann, and C. Freischläger, "On volumetric locking of low-order solid and solid-shell elements for finite elastoviscoplastic deformations and selective reduced integration," *Eng. Comput.*, Apr. 2013.

[6]   N. Büchter and E. Ramm, "Shell theory versus degeneration—a comparison in large rotation finite element analysis," *Int. J. Numer. Methods Eng.*, vol. 34, no. 1, pp. 39–59, Mar. 1992.

[7]   N. Büchter, E. Ramm, and D. Roehl, "Three-dimensional extension of non-linear shell formulation based on the enhanced assumed strain concept," *Int. J. Numer. Methods Eng.*, vol. 37, no. 15, pp. 2551–2568, Aug. 1994.

[8]   N. El-Abbasi and S. A. Meguid, "New shell element accounting for through-thickness deformation," *Comput. Methods Appl. Mech. Eng.*, vol. 189, no. 3, pp. 841–862, 2000.

[9]   P. Betsch, F. Gruttmann, and E. Stein, "A 4-node finite shell element for the implementation of general hyperelastic 3D-elasticity at finite strains," *Comput. Methods Appl. Mech. Eng.*, vol. 130, no. 1–2, pp. 57–79, 1996.

[10]   M. Bischoff and E. Ramm, "Shear deformable shell elements for large strains and rotations," *Int. J. Numer. Methods Eng.*, vol. 40, no. February, pp. 4427–4449, 1997.

[11]   R. P. R. Cardoso and J. W. Yoon, "One point quadrature shell element with through-thickness stretch," *AIP Conf. Proc.*, vol. 778 A, pp. 739–744, 2005.

[12]   T. Lee, M. Leok, and N. H. McClamroch, "Geometric numerical integration for complex dynamics of tethered spacecraft," *Proc. 2011 Am. Control Conf.*, no. March, pp. 1885–1891, 2011.

[13]   S. T. More and R. S. Bindu, "Effect of Mesh Size on Finite Element Analysis of Plate Structure," *Int. J. Eng. Sci. Innov. Technol.*, vol. 4, no. 3, pp. 181–185, 2015.

[14]   L. J. Swys and R. De Borst, "Wave propagation and localization in a rate-dependent cracked medium—model formulation and one-dimensional examples," *Int. J. Solids Struct.*, vol. 29, no. 23, pp. 2945–2958, 1992.

[15]   L. J. Sluys, R. De Borst, and H.-B. Mdhlhaus, "Wave propagation, localization and dispersion in a gradient-dependent medium," *Int. J. Solids Struct.*, vol. 30, no. 9, pp. 1153–1171, 1993.

[16]   R. de Borst, "Damage, Material Instabilities, and Failure," in *Encyclopedia of Computational Mechanics*, Chichester, UK: John Wiley & Sons, Ltd, 2004.

[17]   T. Belytschko, Z. P. Bažant, H. Yul-Woong, and C. Ta-Peng, "Strain-softening materials and finite-element solutions," *Comput. Struct.*, vol. 23, no. 2, pp. 163–180, Jan. 1986.

[18]   D. Lasry and T. Belytschko, "Localization limiters in transient problems," *Int. J. Solids Struct.*, vol. 24, no. 6, pp. 581–597, 1988.

[19]   G. I. Barenblatt, "The Mathematical Theory of Equilibrium Cracks in Brittle Fracture," *Adv. Appl. Mech.*, vol. 7, no. C, pp. 55–129, 1962.

[20]   Z. Bazant and J. Planas, "Fracture and Size Effect in Concrete and other Quasibrittle Materiales," *CRC press LCC, ISBN 0-8493-8284-X°*. CRC Press, p. 616, 1998.

[21]   D. S. Dugdale, "Yielding of steel sheets containing slits," *J. Mech. Phys. Solids*, vol. 8, no. 2, pp. 100–104, May 1960.

[22]   Z. Bazant and B. Oh, "Crack band theory of concrete," *Mater. Struct.*, vol. 16, pp. 155–177, 1983.

[23]   G. Pijaudier-Cabot, Z. P. Bažant, and M. Tabbara, "Comparison of various models for strain-softening," *Eng. Comput.*, vol. 5, no. June, pp. 141–150, 1988.

[24]   Z. Bazant and B. Oh, "Crack band theory of concrete," *Mater. Struct.*, vol. 16, no. 3, pp. 155–177, May 1983.

[25]   R. H. J. Peerlings, R. De Borst, W. A. M. Brekelmans, and J. H. P. de Vree, "Gradient enhanced damage for quasi-brittle materials," *Int. J. Numer. Methods Eng.*, vol. 39, no. 19, pp. 3391–3403, Oct. 1996.

[26]   A. Simone, "Explicit and implicit gradient-enhanced damage models," *Revue Européenne de Génie Civil*, vol. 11, no. 7–8. pp.

1023–1044, Aug-2007.

[27] E. C. Aifantis, "The physics of plastic deformation," *Int. J. Plast.*, vol. 3, no. 3, pp. 211–247, Jan. 1987.

[28] Z. P. Bažant and M. Jirásek, "Nonlocal Integral Formulations of Plasticity and Damage: Survey of Progress," *J. Eng. Mech.*, vol. 128, no. 11, pp. 1119–1149, 2002.

[29] Z. P. Bažant, "Mechanics of Distributed Cracking," *Appl. Mech. Rev.*, vol. 39, no. 5, p. 675, 1986.

[30] D. a. Pecknold and S. Rahman, "Micromechanics-based structural analysis of thick laminated composites," *Comput. Struct.*, vol. 51, no. 2, pp. 163–179, 1994.

[31] A. Tabiei, W. Yi, and R. Goldberg, "Non-linear strain rate dependent micro-mechanical composite material model for finite element impact and crashworthiness simulation," *Int. J. Non. Linear. Mech.*, vol. 40, no. 7, pp. 957–970, 2005.

[32] A. Tabiei and S. B. Aminjikarai, "A strain-rate dependent micro-mechanical model with progressive post-failure behavior for predicting impact response of unidirectional composite laminates," *Compos. Struct.*, vol. 88, no. 1, pp. 65–82, 2009.

[33] A. Tabiei and Q. Chen, "Micromechanics Based Composite Material Model for Crashworthiness Explicit Finite Element Simulation," *J. Thermoplast. Compos. Mater.*, vol. 14, no. 4, pp. 264–289, 2001.

[34] S. Medikonda, A. Tabiei, and R. Hamm, "A Comparative study on the Effect of Representative Volume Cell (RVC) Boundary Conditions on the Elastic Properties of a Micromechanics Based Unidirectional Composite Material Model," *Int. J. Compos. Mater.*, vol. 7, no. 2, pp. 51–71, 2017.

[35] S. Medikonda and A. Tabiei, "A nonlinear strain rate and pressure-dependent micro-mechanical composite material model for impact problems," *J. Thermoplast. Compos. Mater.*, p. 892705717744329, 2017.

[36] R. K. Goldberg, G. D. Roberts, and A. Gilat, "Implementation of an Associative Flow Rule Including Hydrostatic Stress Effects into the High Strain Rate Deformation Analysis of Polymer Matrix Composites," *J. Aerosp. Eng.*, vol. 18, no. 1, pp. 18–27, 2005.

[37] X. Zheng and W. K. Binienda, "Rate-Dependent Shell Element Composite Material Model Implementation in LS-DYNA," *J. Aerosp. Eng.*, vol. 21, no. 3, pp. 140–151, Jul. 2008.

[38] J. Qu and M. Cherkaoui, "Effective Properties of Fiber-Reinforced Composite Laminates," in *Fundamentals of Micromechanics of Solids*, Hoboken, NJ, USA: John Wiley & Sons, Inc., 2006, pp. 214–244.

[39] LSTC, *LS-DYNA Keyword User's Manual Volume II R7.1*, vol. II. 2014.

[40] C.-F. Yen and A. P. Ground, "A ballistic material model for continuous - fiber reinforced composites," *Int. J. Impact Eng.*, vol. 46, no. August, pp. 11–22, 2012.

[41] L. Murray, Y. and Schwer, "Implementation and Verification of the Fiber Composite Damage Models," *Fail. Criteria Anal. Dyn. Response; ASME AMD*, vol. 107, pp. 21–30, 1990.

[42] J. Van Hoof, M. J. Worswick, P. V Straznicky, M. Bolduc, and S. Tylko, "Simulation of the ballistic impact response of composite helmets," in *Proceedings of the 5th international LS-DYNA users conference*, 1998.

[43] A. Matzenmiller, J. Lubliner, and R. L. Taylor, "A constitutive model for anisotropic damage in fiber-composites," *Mech. Mater.*, vol. 20, no. 2, pp. 125–152, 1995.

[44] K. V Williams and R. Vaziri, "Application of a damage mechanics model for predicting the impact response of composite materials," *Comput. Struct.*, vol. 79, no. 10, pp. 997–1011, 2001.

[45] K. V. Williams, R. Vaziri, and A. Poursartip, "A physically based continuum damage mechanics model for thin laminated composite structures," *Int. J. Solids Struct.*, vol. 40, no. 9, pp. 2267–2300, 2003.

[46] F. Andrade, M. Vogler, J. Cesar de Sa, and F. Andrade Pires, "User-Defined Nonlocal Models in LS-DYNA," *8th Eur. LS-DYNA User Conferece*, 2011.

[47] S. Babu Aminjikarai and A. Tabiei, "A strain-rate dependent 3-D micromechanical model for finite element simulations of plain weave composite structures," *Compos. Struct.*, vol. 81, no. 3, pp. 407–418, Dec. 2007.

[48] N. Stander, W. Roux, A. Basudhar, T. Eggleston, T. Goel, and K. Craig, *LS-OPT User's Manual - A Design Optimization and Probabilistic Analysis Tool*, no. December. 2015.

[49] D. Delfosse, A. Poursartip, B. R. Coxon, and E. F. Dost, "Non-penetrating impact behavior of CFRP at low and intermediate velocities," *Proc. 5th Symp. Compos. Mater. Fatigue Fract. May 4, 1993 - May 6*, no. 1230, pp. 333–350, 1995.

[50] G. A. O. Davies and X. Zhang, "Impact damage prediction in carbon composite structures," *Int. J. Impact Eng.*, vol. 16, no. 1, pp. 149–170, Feb. 1995.